Magnetic Adsorbents for Selective Removal of Selenite from Contaminated Water

Samuel F. Evans, [†,‡] Marko R. Ivancevic, [†] Jiaqiang Yan, [⊥] Amit K. Naskar, [†,‡] Alan M. Levine,[#] Richard J. Lee, [#] Costas Tsouris, [+] M. Parans Paranthaman, [†,‡,*]

[†] Chemical Sciences Division, Oak Ridge National Laboratory, Oak Ridge, Tennessee 37831, USA

[‡] The Bredesen Center for Interdisciplinary Research and Graduate Education, The University of Tennessee, Knoxville, Tennessee 37996, USA

[⊥] Materials Science and Technology Division, Oak Ridge National Laboratory, Oak Ridge, Tennessee 37831, USA

[#] RJ Lee Group, Monroeville, Pennsylvania 15146, USA

[+] Energy and Transportation Science Division, Oak Ridge National Laboratory, Oak Ridge, Tennessee 37831, USA

Correspondence to: M. Parans Paranthaman (paranthamanm@ornl.gov)

Abstract

Novel meso- and microporous tire-derived carbon framework as a support for magnetic iron oxide nanoparticle adsorbents (MNA) that selectively adsorb selenite (Se(IV)) ions from contaminated water has been developed. Carbon supported magnetic nanoparticle adsorbents (C-MNA) displayed higher adsorption values compared to MNA from 5 - 50 ppm selenite concentrations, maximizing at 48±5 mg/g capacity with > 99% Se removal at pH 3 and 5, and outperforms MNA at pH 7. These improvements will expand the range of water sources that can be treated, as well as easing adsorbent collection through magnetic separation.

Keywords: Selenium removal, tire derived carbon support, iron oxide magnetic nanoparticles, adsorbents, water treatments.

I. Introduction

Water availability and sourcing are becoming ever more important for society as growing populations increase demand for potable and irrigation water. Pollution of water sources has and continues to be a threat to human health and the environment. This problem is expected to worsen as clean water demand increases with population. Before use, water must meet guidelines set by the US Environmental Protection Agency (EPA), European Union, World Health Organization or other regulatory agencies depending on the location. This is due to the multitude of inorganic, organic, biological, and particulate contaminants that can be present in water that poses serious health and environmental hazards. Among these contaminants are selenium, a naturally occurring contaminant that is commonly present in natural water environments, at pH 3-8, as protonated selenite (SeO_3^{2-}), and selenate (SeO_4^{2-}) salt ions.[1] Selenium is one such pollutant that is highly toxic to humans and animals, so removal to regulated exposure levels is critical. In solution these ions will exist as anionic species or protonated species depending on the pH of the contaminated water stream.[2] While selenium is a necessary supplement, overexposure is dangerous and potentially fatal. Selenite and selenate have been found to be quite toxic, with doses of 1.5-6 mg/kg of body weight leading to death.[3] The danger is exacerbated when the heavy metal is leached into a water supply, which commonly occurs in various regions of the USA such as South Dakota, in addition to areas of China. Typical water concentrations in areas with high amounts of selenium containing minerals can reach up to 4.2 ppm.[4] In addition to these contaminated areas mining wastewater can accumulate selenium to concentrations of 2.2 ppm, both values far exceeding recommended exposure limits.[5] With such a high toxicity at such low concentrations, and the prevalence of selenium in the environment investigations into efficient removal of selenium has been explored extensively.[2, 6, 7]

Methods developed to remove selenium includes treatments with various adsorbents including metal oxides,[8] magnetic nanoparticles,[9] layered double hydroxides,[10] mesoporous materials,[11, 12], metal-organic frameworks (MOFs),[13] MgO nanosheets,[14] carbon-nanotubes,[15] and bioremediation based methods.[16-18] Ion exchange resins have also been explored as low-cost adsorbents and they have been used in conjunction with reverse osmosis, which adds additional energy requirements to the process.[3] Adsorption is the primary mechanism utilized for selenium removal, which prompted an investigation into the use of environmentally friendly and economically sustainable materials for this method.

Researchers at Oak Ridge National Laboratory have developed a method for converting waste car tires into a uniquely micro- and mesoporous carbon black material.[19-21] Recycling of tire-waste is of great importance due to the health hazards and environmental cost from improper disposal. When tire waste is placed in landfills, chemical additives from their production can leach into the environment, causing damage. Other reprocessing methods, such as burning for energy, creates further problems with air pollution.[22] Tire-derived carbon has displayed promise for Li, Na, and K-ion battery materials,[21, 23-26] pseudo-capacitors,[27, 28] biofuel conversion,[29-31] and, electrocatalysis.[32] Previous work on biofuel catalysis prompted our investigation into the present work on materials for water treatment. Use of porous carbon as a support[33, 34] and functionalized material[35-37] for catalysis, energy, and environmental applications has been well studied. Bio-derived and waste material carbon precursors are widely explored for their sustainability, cost-savings and comparable performance to engineered carbon alternatives. Previous studies have also shown sulfonated carbon and tire-derived carbon's ability to remove organic dye pollutants effectively.[38, 39]

Herein, a new adsorbent using waste tire-derived mesoporous carbon infiltrated with iron oxide nanoparticles was developed. This carbon-supported magnetic nanoparticle adsorbent (C-MNA) was compared with existing selenium adsorption materials, referred to as magnetic nanoparticle adsorbents (MNA). C-MNA was found to meet the treatment standards of the EPA for selenium contamination in water (≤ 50 ppb) due to a variety of factors. The unique porosity and hierarchy of pore distribution found in the activated tire carbon promotes easy infiltration of MNA. This infiltration improved MNA stability over time, prevented agglomeration during synthesis, increased selenium adsorption of C-MNA, and increased the selenium adsorption pH range of the sorbent. These improved properties were also complemented by selective adsorption of selenite (Se(IV)), over selenate (Se(VI)). Improving the durability and operating range of selenium adsorbents in addition to the use of inexpensive precursors and materials will allow for expanded environmental cleanup options. While hard carbon, and FeNP are both known to interact with other metal ions, anions, and organics[40-43] in aqueous solution but is considered out of the scope to the current research on selenium removal. Additionally, the magnetic properties of the material allow for removal by magnetic separation, improving recovery and reusability of the C-MNA, as seen in the proposed process flow in Figure 1.

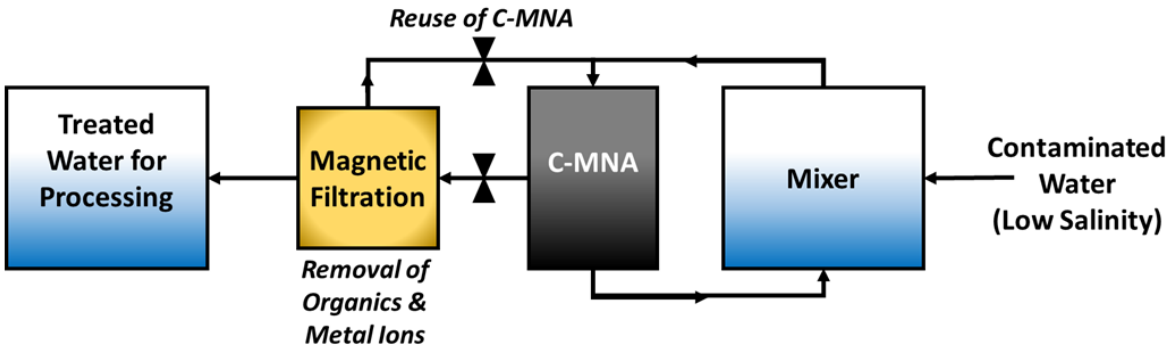

Figure 1. Schematic of heavy metal removal step with carbon supported iron oxide magnetic nanoparticle adsorbents, C-MNA in a water treatment process.

II. Experimental Methods

II.1 Carbon Synthesis

Tire-derived carbon was synthesized as previously described.[20] The surface area of the carbon was increased by chemical treatment with KOH (Sigma Aldrich, ≥85%) in a 1:4 ratio, followed by pyrolysis at 800 °C for 1 h in a flowing nitrogen atmosphere with a ramp rate of 10 °C/min.[19]

II.2 C-MNA and MNA synthesis

For C-MNA synthesis, carbon material was dispersed in the aqueous solution containing $FeCl_3$ (Sigma-Aldrich, 97% purity) and $FeSO_4$ (Sigma-Aldrich, ≥99% purity) in a 6:5 mole ratio of Fe(III) and Fe(II). The solution was stirred for one hour, then heated to 70 °C. 1M NaOH (Alfa Aesar, pellets, 98% purity) was then added to the solution to initiate precipitation of MNA. Here the suspension of carbon in solution allowed for the infiltration of MNA into the meso- and micropores of the carbon. After precipitation, the solution was filtered with microfilter paper, retaining the larger C-MNA particles and removing residual starting material and synthesized MNA.

MNA was synthesized based on the established procedures[44] for comparison to C-MNA. Iron precursor and precipitation solutions and procedure were identical to C-MNA. Precipitated MNA were centrifuged for separation. Particles were held by a sintered magnet and rinsed with DI water to remove any residual starting materials and completely neutralize the pH of the samples, then oven dried in air.

II.3 Characterization

X-ray diffraction (XRD) patterns were collected on a PANalytical Empyrean with a Cu Kα radiation. All data were processed with HighScore Plus. Inductively coupled plasma optical emission spectroscopy (ICP-OES) compositional analysis was performed to determine selenite removal from the solution using a Thermo Fisher iCAP Model 7400 ICP-OES Duo. The ICP-OES has a minimum selenium detection limit of 0.77 µg/L at a wavelength of 196 nm. During measurements the linear standard curve had an R^2 value of 1 and a limit of detection of 0.049 ppm. For the calculation of iron content the ICP-OES has a minimum detection limit of 0.15 µg/L at a wavelength of 260 nm. During measurements the linear standard curve had an R^2 value of 0.996 and a limit of detection of 2.683 ppm. Magnetic properties were measured with a Quantum Design (QD) Magnetic Property Measurement System at room temperature. A Zeiss Merlin VP scanning electron microscope (SEM) operated at 3 kV and a Hitachi HD-2300A scanning transmission electron microscope (STEM) with a field emission source operated at 200 kV in bright-field imaging mode at a 2.1 Å resolution, were used to characterize the surface morphologies of the samples.

II.4 Selenium adsorption tests

Selenium adsorption tests were performed with simulated contaminated water (high purity DI water, >18MΩ) in a 5mL solution containing sodium selenite (Sigma, Bioreagent, ≥98% purity) or sodium selenate (Sigma, Bioxtra) and 20mg of adsorbent. Trials were performed with a sample shaker to ensure uniform stirring for differing times. Removal of selenium was determined by the difference between the starting concentration of the solution and the final concentration with ICP-OES analysis. For statistical accuracy ICP-OES samples were measured in triplicate through the instrument software in addition to undergoing multiple repeat analyses,

Figures 1 and 2 display the standard deviations of these measurements with error bars. Desorption can be carried out through mixing with a 0.025 molar NaOH solution. During tests, full desorption to starting selenium values was observed. Percent removal and mass of selenium adsorbed per gram of sorbent were then calculated using equations 1 and 2.

$$Capacity = \frac{(C_{Se,i} - C_{Se,f}) * V}{m_{Adsorbent}} \quad (1)$$

$$Percent\ removal = 100 * \left(\frac{C_{Se,i} - C_{Se,f}}{C_{Se,i}}\right) \quad (2)$$

Where $C_{Se,i}$ is the initial concentration of selenium, $C_{Se,f}$ is the final concentration of selenium post testing, V is the volume of sample used, and $m_{Adsorbent}$ is the mass of the C-MNA or MNA used in the sample.

Determination of maximum adsorption by time, selenite concentration dependence, and pH dependence were all performed by the described procedure. Adsorption dependence with time was determined by mixing the adsorbents for 0.25, 0.5, 0.75, 1, 4, and 24 h. Selenite concentrations of 5, 10, 25, and 50 ppm were tested. The pH dependence of the adsorbents was tested for 3, 5, 7, 9, and 11 at a selenite concentration of 5 ppm. pH was adjusted using 1M NaOH and HCl solutions.

III. Results and Discussion

C-MNA and MNA underwent a variety of selenium removal tests to determine adsorbent performance. Initial testing exhibited complete selectivity for selenite (Se(IV)) over selenate (Se(VI)), with no adsorption observed through ICP-OES. Selenite species have ten times the toxicity of selenates,[45] so selective removal would be beneficial.[2] Carbon based sorbents are also known to perform physisorption of selenite species. The carbon support here is known to

have residual acidic sulfonyl groups, $(SO_4)^{2-}$. These groups, depending on the pH of the solution may enhance or inhibit selenite uptake as electrostatic interaction will dictate uptake of sulfonyl and FeNPs. Removal of selenite species is known to occur from the interaction of the charged SeO_3^{2-} with surface FeOH and FeH^{2+} groups of magnetite nanoparticles.[46] Investigation into the effect of time on adsorption found maximum selenite uptake after 30 min of agitation, as seen in Figure 2. After this initial peak adsorption at 30 min competition between physisorption of the carbon and chemisorption of sulfonyl and FeNP groups leads to a drop in adsorption which does not recover until 24 hours later.

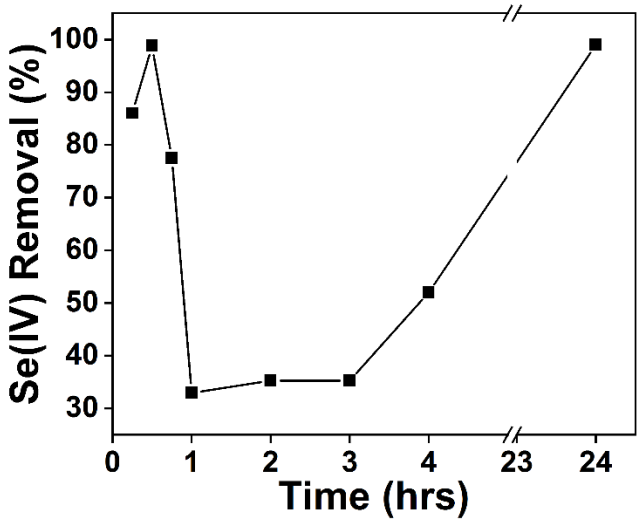

Figure 2. Determination of effective solution contact time of adsorbents at pH 5 with a simulated 5 ppm selenite.

After determining peak selenite adsorption occurred after 30 min, the pH dependence of C-MNA was compared with MNA. Figure 3 displays comparable selenite removal at pH 3 and 5 between C-MNA and MNA. C-MNA shows improved adsorption performance at pH 7 and once again comparable removal at pH 9. Once higher pH has been reached, C-MNA and MNA become ineffective at removing any selenite, dropping to 0 percent removal. Selenite removal tests were

performed over a range of pH to determine if the porous carbon support provided any benefits to the MNAs in terms of adsorption or protection from degradation. Before the maximum uptake capacities of C-MNA and MNA were determined, the mass loading of FeNP within the carbon support was calculated to display adsorption on a mg/g FeNP basis. Upon dissolution in acid and analysis by ICP-OES the weight percent of FeNP was found to be 17% in C-MNA. Control tests with only the carbon support resulted in a maximum of 1.52±0.01 mg/g selenite adsorption. This corresponds to no more than 16% adsorption performed by physisorption of the support. The bulk of the adsorption is performed by chemisorption from the intercalated FeNPs. To determine the maximum selenite uptake of C-MNA, trials were performed with 5, 10, 25, 50 ppm selenite concentrations at pH 5. Figure 4 displays the resulting adsorption capacity values, with a maximum of 47.8±5.0 mg/g for 50 ppm. Selenium concentration in contaminated sites is generally much lower from 10 ppm to less than 1 ppm.[2] Here adsorption capacity for 5 ppm Se(IV) concentration, 5.59±0.02 mg/g, is more pertinent to real-world conditions. Compared to existing selenium adsorbents, reported in Table 1, C-MNA exhibits improved performance compared to oxide materials and bioremediation methods. Few bioremediation methods and MOF materials surpass C-MNA's adsorption. These methods also have a cost disadvantages for various reasons including more complex synthesis route in the case of MOF materials, and material costs for the growth and maintenance of bioremediation cultures. This is promising as C-MNA's low cost and ease of preparation competes well with existing materials, in addition to forming value-added materials derived from the waste material .

Table 1. Selenite uptake capacities of different adsorbent material. *Adsorption capacity is calculated based on the active material content (FeNP determined by ICP-OES).

Adsorbent	Selenite Concentration (ppm)	Selenite Capacity (mg/g)	Ref.
Binary Oxide Fe(III)/SiO_2	10	20.4	[9]
Binary Oxide Al(III)/SiO_2	10	32.7	
S. cerevisiae dried biomass	50	39.02	[16]
Cladophora hutchinsiae (green algae)	10-400	74.9	[17]
MOF NU-1000	1	95	[13]
G. lucidum mushroom	20-140	127	[18]
MNA	**50**	**7.53**	**This work**
C-MNA	**5**	**5.6***	
	50	**47.8***	

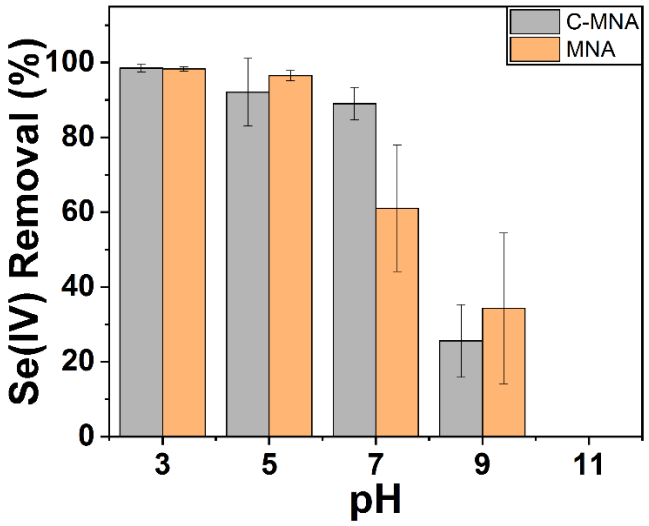

Figure 3. Percent Se(IV) removal with C-MNA and MNA at pH 3, 5, 7, 9, and 11 with 20 mg of adsorbent in 5 mL of simulated contaminated water (5 ppm selenite) over 30 min.

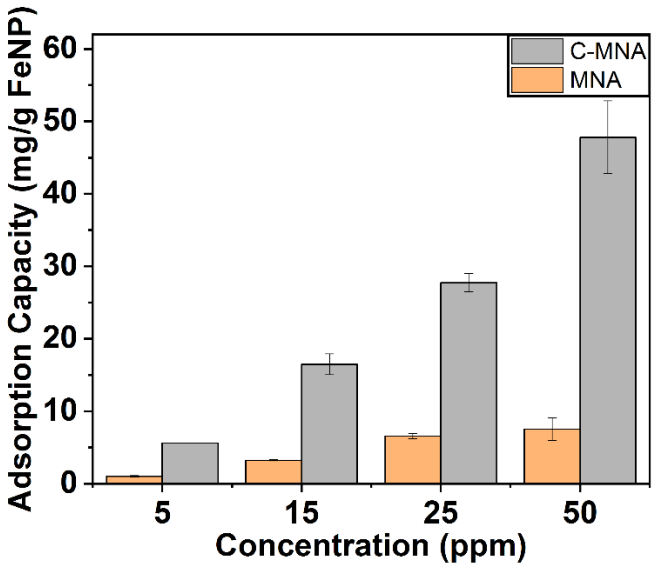

Figure 4. Se(IV) adsorption capacity of C-MNA and MNA from 5, 10, 25, and 50 ppm concentration solutions. The tests were run at pH 5 with a 4:1 adsorbent mass to selenite solution volume over 30 min.

Removal tests over a range of pH displayed C-MNA's improved performance at neutral pH. This is thought to come between the competition of OH^-, SeO_3^{2-} and $HSeO_3^-$ in solution from adsorbing to MNAs.[9] The carbon framework of C-MNA offers some protection to internal MNA from OH^- resulting in improved selenium removal at pH 7. Since selenite contamination occurs in acidic to slightly basic (≤ 8 pH) water environments, the introduction of a carbon support is beneficial to extend the range of environments that can be treated. Also, C-MNA can be removed along with Se impurities by magnetic separation and then regenerated by desorbing selenium with a 0.025 M NaOH solution.

Figure 5 compares the field dependence magnetization of C-MNA, and MNA at room temperature both of which exhibit superparamagnetic behavior. Additionally, C-MNA has a magnetic moment almost three times the magnitude of the MNA. This is unexpected considering that carbon-support reduces the volume fraction of magnetic nanoparticles in C-MNA. This is

thought to arise from the controlled precipitation of magnetic nanoparticles in the hierarchical meso- and micropore structure, which allows for the orientation of magnetic moments. Further, the restricted size of the pores within the carbon support could promote the formation of different particle sizes of FeNP, which have been shown to affect the magnetic moments.[47] During synthesis MNA does not have this size restriction, making particle formation rapid and the orientation of magnetic moments less ordered. In addition, the formation of FeO(OH) groups, which have a smaller magnetic moment than Fe_3O_4,[48, 49] resulting from degradation due to exposure in air may also contribute to the difference in the magnetic moments over time. C-MNA is comparable with other magnetite-based adsorbents which range from 20-60 emu/g for magnetic hysteresis measurements.[9, 50]

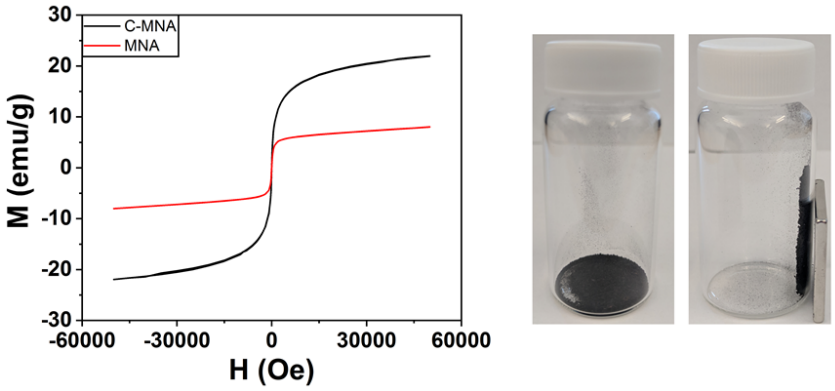

Figure 5. Magnetic properties of C-MNA and MNA. An increase in the strength of magnetic moments from C-MNA to MNA was observed. Photo of C-MNA placed in a vial without and with a sintered magnet on the side. The picture on the right demonstrates C-MNA's response to a magnet.

Analysis by XRD in Figure 6(a) shows the presence of amorphous carbon and magnetite, Fe_3O_4, peaks in C-MNA. After exposure to ambient conditions over 30 days, the FeNPs remained stable due to the carbon scaffolding. In Figure 6(b), MNA particles contain mainly the Fe_3O_4 phase. However, after exposure to ambient conditions over 30 days, MNA partially degraded to a

FeO(OH) phase, this is thought to occur from interaction with air and moisture.[51] Figure 7(a) displays the underlying carbon structure that allows for nucleation of MNA within the carbon. This is further corroborated by elemental mapping in Figure 7(c). Successful precipitation of MNA into the porous carbon framework was thought to improve their stability to degradation over time. Previous work has shown that the carbon undergoes a decrease in surface area upon the incorporation of iron species within the internal pore network.[30] The addition of a carbon structural support also suppressed the agglomeration of MNA, increasing active surface area for Se(IV) adsorption. Figure 7(c) displays the distribution of Fe in carbon. Figures 7(b) and (d) show the agglomeration of smaller nanoparticles, on the order of tens of nanometers, into larger micron sized structures. In Figure 7(d), the presence of carbon on the surface of MNA occurs from surface adsorption of atmospheric CO_2 with FeO(OH) surface species.[52] Without the presence of a carbon support FeNPs randomly orient, leading to a smaller magnetic moment as well as the formation of undesired species such as FeO(OH). By promoting FeNP precipitation within the carbon support, adsorption capacity and FeNP adsorption efficiency can be maximized.

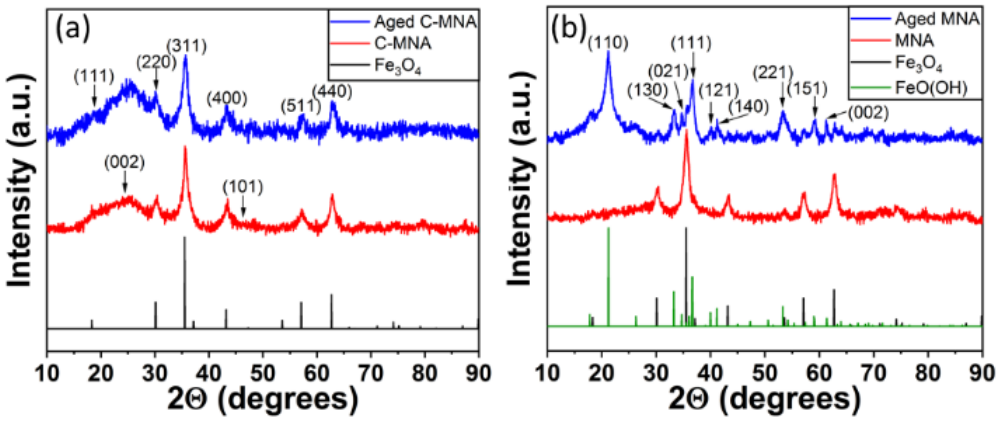

Figure 6. X-ray diffraction (XRD) patterns of (a) C-MNA; and (b) MNA particles exposed (aged) over one month in ambient conditions. Fe_3O_4 and amorphous carbon peaks are displayed in (a) and FeO(OH) in (b). MNA undergoes a loss of the magnetite phase and formation of a

FeO(OH) phase from oxidation. C-MNA does not undergo this change due to carbon scaffolding.

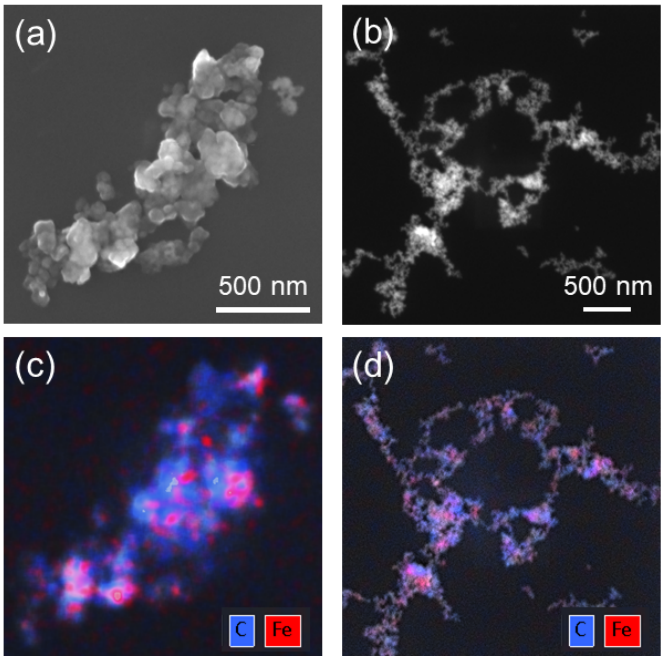

Figure 7. SEM image of the surface of (a) C-MNA, (b) MNA particles with elemental mapping of C and Fe in (c) C-MNA and (d) MNA.

IV. Conclusions

Here tire-derived carbon is shown to be an effective protective support for iron oxide based magnetic nano adsorbents. Incorporation of nanoparticles into the meso- and micropores of C-MNA provides stability from degradation and agglomeration in ambient conditions. Internal precipitation of MNAs into carbon also improved magnetic properties, total selenite uptake capacity at a variety of concentrations and expanded performance at pH 7 compared to MNA. The low cost of the iron oxide precursors and tire-derived carbon contributes significantly to the reduced costs associated with producing selenite adsorbents. Carbon supported magnetic nanoparticle adsorbents allow for effective magnetic separation of adsorbents with Se from

treatment solutions. Interaction of the carbon support and FeNP with other anions, metals, and organics in solution is expected and will be the subject of further study in addition to scale-up studies of magnetic separation. These added benefits will help make water treatment more cost-effective and expand the range of contaminated water sources that can be treated.

ASSOCIATED CONTENT

AUTHOR INFORMATION

Corresponding authors

*Phone (865) 574-5045; email: paranthamanm@ornl.gov

ORCID # 0000-0003-3009-8531

Notes

The authors declare no competing financial interest.

ACKNOWLEDGEMENTS

The carbon synthesis research (MPP) was supported by the U.S. Department of Energy (DOE), Office of Science, Office of Basic Energy Sciences, Materials Sciences and Engineering Division. SFE is grateful for a fellowship from the Bredesen Center for Interdisciplinary Graduate Education. CT was supported by the Laboratory Directed Research and Development (LDRD) program of the Oak Ridge National Laboratory. Magnetic property measurements (JQY) was supported by the U.S. Department of Energy (DOE), Office of Science, Basic Energy Sciences, Materials Sciences and Engineering Division

This manuscript has been authored by UT-Battelle, LLC under Contract No. DE-AC05-00OR22725 with the US DOE. The U.S. Government retains and the publisher, by accepting the

References

(1) Torres, J.; Pintos, V.; Gonzatto, L.; Domínguez, S.; Kremer, C.; Kremer, E. (2011) Selenium chemical speciation in natural waters: Protonation and complexation behavior of selenite and selenate in the presence of environmentally relevant cations. *Chemical Geology*, 288(1-2): 32-38.

(2) Santos, S.; Ungureanu, G.; Boaventura, R.; Botelho, C. (2015) Selenium contaminated waters: An overview of analytical methods, treatment options and recent advances in sorption methods. *Sci Total Environ*, 521-522: 246-260.

(3) Edition, F. (2011) Guidelines for drinking-water quality. *WHO chronicle*, 38(4): 104-108.

(4) Fordyce, F.M. (2013) Selenium Deficiency and Toxicity in the Environment in Selinus, O. (Ed) *Essentials of Medical Geology: Revised Edition*;Springer Netherlands:Dordrecht

(5) Khamkhash, A.; Srivastava, V.; Ghosh, T.; Akdogan, G.; Ganguli, R.; Aggarwal, S. (2017) Mining-Related Selenium Contamination in Alaska, and the State of Current Knowledge. *Minerals*, 7(3).

(6) Frankenberger, W.T.; Arshad, M. (2001) Bioremediation of selenium-contaminated sediments and water. *BioFactors*, 14(1-4): 241-254.

(7) Fu, F.; Cheng, Z.; Lu, J. (2015) Synthesis and use of bimetals and bimetal oxides in contaminants removal from water: a review. *RSC Advances*, 5(104): 85395-85409.

(8) Peak, D. (2006) Adsorption mechanisms of selenium oxyanions at the aluminum oxide/water interface. *J Colloid Interface Sci*, 303(2): 337-345.

(9) Sun, W.; Pan, W.; Wang, F.; Xu, N. (2015) Removal of Se(IV) and Se(VI) by MFe2O4 nanoparticles from aqueous solution. *Chemical Engineering Journal*, 273: 353-362.

(10) Asiabi, H.; Yamini, Y.; Shamsayei, M. (2017) Highly selective and efficient removal of arsenic(V), chromium(VI) and selenium(VI) oxyanions by layered double hydroxide intercalated with zwitterionic glycine. *J Hazard Mater*, 339: 239-247.

(11) Jegadeesan, G.; Mondal, K.; Lalvani, S.B. (2003) Comparative study of selenite adsorption on carbon based adsorbents and activated alumina. *Environ Technol*, 24(8): 1049-1059.

(12) Rabiul Awual, M.; Munjur Hasan, M.; Ihara, T.; Yaita, T. (2014) Mesoporous silica based novel conjugate adsorbent for efficient selenium(IV) detection and removal from water. *Microporous and Mesoporous Materials*, 197: 331-338.

(13) Howarth, A.J.; Katz, M.J.; Wang, T.C.; Platero-Prats, A.E.; Chapman, K.W.; Hupp, J.T.; Farha, O.K. (2015) High efficiency adsorption and removal of selenate and selenite from water using metal-organic frameworks. *J Am Chem Soc*, 137(23): 7488-7494.

(14) Cui, W.; Li, P.; Wang, Z.; Zheng, S.; Zhang, Y. (2018) Adsorption study of selenium ions from aqueous solutions using MgO nanosheets synthesized by ultrasonic method. *J Hazard Mater*, 341: 268-276.

(15) Vilardi, G.; Mpouras, T.; Dermatas, D.; Verdone, N.; Polydera, A.; Di Palma, L. (2018) Nanomaterials application for heavy metals recovery from polluted water: The combination of nano zero-valent iron and carbon nanotubes. Competitive adsorption non-linear modeling. *Chemosphere*, 201: 716-729.

(16) Khakpour, H.; Younesi, H.; Mohammadhosseini, M. (2014) Two-stage biosorption of selenium from aqueous solution using dried biomass of the baker's yeast Saccharomyces cerevisiae. *Journal of Environmental Chemical Engineering*, 2(1): 532-542.

(17) Tuzen, M.; Sarı, A. (2010) Biosorption of selenium from aqueous solution by green algae (Cladophora hutchinsiae) biomass: Equilibrium, thermodynamic and kinetic studies. *Chemical Engineering Journal*, 158(2): 200-206.

(18) Nettem, K.; Almusallam, A.S. (2013) Equilibrium, Kinetic, and Thermodynamic Studies on the Biosorption of Selenium (IV) Ions ontoGanoderma LucidumBiomass. *Separation Science and Technology*, 48(15): 2293-2301.

(19) Li, Y.; Cheng, Y.; Daemen, L.L.; Veith, G.M.; Levine, A.M.; Lee, R.J.; Mahurin, S.M.; Dai, S.; Naskar, A.K.; Paranthaman, M.P. (2017) Neutron vibrational spectroscopic studies of novel tire-derived carbon materials. *Phys Chem Chem Phys*, 19(33): 22256-22262.

(20) Naskar, A.K.; Paranthaman, M.P.; Bi, Z., Pyrolytic carbon black composite and method of making the same. In Google Patents: 2016.

(21) Naskar, A.K.; Bi, Z.; Li, Y.; Akato, S.K.; Saha, D.; Chi, M.; Bridges, C.A.; Paranthaman, M.P. (2014) Tailored recovery of carbons from waste tires for enhanced performance as anodes in lithium-ion batteries. *RSC Advances*, 4(72).

(22) Adhikari, B. (2000) Reclamation and recycling of waste rubber. *Progress in Polymer Science*, 25(7): 909-948.

(23) Li, Y.; Paranthaman, M.P.; Akato, K.; Naskar, A.K.; Levine, A.M.; Lee, R.J.; Kim, S.-O.; Zhang, J.; Dai, S.; Manthiram, A. (2016) Tire-derived carbon composite anodes for sodium-ion batteries. *Journal of Power Sources*, 316: 232-238.

(24) Li, Y.; Adams, R.A.; Arora, A.; Pol, V.G.; Levine, A.M.; Lee, R.J.; Akato, K.; Naskar, A.K.; Paranthaman, M.P. (2017) Sustainable Potassium-Ion Battery Anodes Derived from Waste-Tire Rubber. *Journal of The Electrochemical Society*, 164(6): A1234-A1238.

(25) Gnanaraj, J.; Lee, R.; Levine, A.; Wistrom, J.; Wistrom, S.; Li, Y.; Li, J.; Akato, K.; Naskar, A.; Paranthaman, M. (2018) Sustainable Waste Tire Derived Carbon Material as a Potential Anode for Lithium-Ion Batteries. *Sustainability*, 10(8).

(26) Li, Y.; Levine, A.M.; Zhang, J.; Lee, R.J.; Naskar, A.K.; Dai, S.; Paranthaman, M.P. (2018) Carbon/tin oxide composite electrodes for improved lithium-ion batteries. *Journal of Applied Electrochemistry*, 48(7): 811-817.

(27) Boota, M.; Paranthaman, M.P.; Naskar, A.K.; Li, Y.; Akato, K.; Gogotsi, Y. (2015) Waste Tire Derived Carbon-Polymer Composite Paper as Pseudocapacitive Electrode with Long Cycle Life. *ChemSusChem*, 8(21): 3576-3581.

(28) Naskar, A.K.; Paranthaman, M.P.; Boota, M.; Gogotsi, Y., Flexible and conductive waste tire-derived carbon/polymer composite paper as pseudocapacitive electrode. In Google Patents: 2018.

(29) Hood, Z.D.; Adhikari, S.P.; Li, Y.; Naskar, A.K.; Figueroa-Cosme, L.; Xia, Y.; Chi, M.; Wright, M.W.; Lachgar, A.; Paranthaman, M.P. (2017) Novel Acid Catalysts from Waste-Tire-Derived Carbon: Application in Waste-to-Biofuel Conversion. *ChemistrySelect*, 2(18): 4975-4982.

(30) Hood, Z.D.; Adhikari, S.P.; Evans, S.F.; Wang, H.; Li, Y.; Naskar, A.K.; Chi, M.; Lachgar, A.; Paranthaman, M.P. (2018) Tire-derived carbon for catalytic preparation of biofuels from feedstocks containing free fatty acids. *Carbon Resources Conversion*, 1(2): 165-173.

(31) Hood, Z.D.; Adhikari, S.P.; Wright, M.W.; Lachgar, A.; Li, Y.; Naskar, A.K.; Paranthaman, M.P., Surface treated carbon catalysts produced from waste tires for fatty acids to biofuel conversion. In Google Patents: 2018.

(32) Hood, Z.D.; Yang, X.; Li, Y.; Naskar, A.K.; Chi, M.; Paranthaman, M.P. (2018) Conversion of Waste Tire Rubber into High-Value-Added Carbon Supports for Electrocatalysis. *Journal of The Electrochemical Society*, 165(14): H881-H888.

(33) Yang, X.Y.; Chen, L.H.; Li, Y.; Rooke, J.C.; Sanchez, C.; Su, B.L. (2017) Hierarchically porous materials: synthesis strategies and structure design. *Chem Soc Rev*, 46(2): 481-558.

(34) Yang, Y.; Chiang, K.; Burke, N. (2011) Porous carbon-supported catalysts for energy and environmental applications: A short review. *Catalysis Today*, 178(1): 197-205.

(35) Stein, A.; Wang, Z.; Fierke, M.A. (2009) Functionalization of Porous Carbon Materials with Designed Pore Architecture. *Advanced Materials*, 21(3): 265-293.

(36) Oschatz, M.; Walczak, R. (2018) Crucial Factors for the Application of Functional Nanoporous Carbon-Based Materials in Energy and Environmental Applications. *C*, 4(4).

(37) Kiciński, W.; Szala, M.; Bystrzejewski, M. (2014) Sulfur-doped porous carbons: Synthesis and applications. *Carbon*, 68: 1-32.

(38) Islam, M.T.; Saenz-Arana, R.; Hernandez, C.; Guinto, T.; Ahsan, M.A.; Bragg, D.T.; Wang, H.; Alvarado-Tenorio, B.; Noveron, J.C. (2018) Conversion of waste tire rubber into a high-capacity adsorbent for the removal of methylene blue, methyl orange, and tetracycline from water. *Journal of Environmental Chemical Engineering*, 6(2): 3070-3082.

(39) Islam, M.T.; Hernandez, C.; Ahsan, M.A.; Pardo, A.; Wang, H.; Noveron, J.C. (2017) Sulfonated resorcinol-formaldehyde microspheres as high-capacity regenerable adsorbent for the

removal of organic dyes from water. *Journal of Environmental Chemical Engineering*, 5(5): 5270-5279.

(40) Wu, Z.; Zhao, D. (2011) Ordered mesoporous materials as adsorbents. *Chem Commun (Camb)*, 47(12): 3332-3338.

(41) Ma, Z.; Shan, C.; Liang, J.; Tong, M. (2018) Efficient adsorption of Selenium(IV) from water by hematite modified magnetic nanoparticles. *Chemosphere*, 193: 134-141.

(42) Huang, S.H.; Chen, D.H. (2009) Rapid removal of heavy metal cations and anions from aqueous solutions by an amino-functionalized magnetic nano-adsorbent. *J Hazard Mater*, 163(1): 174-179.

(43) Xu, P.; Zeng, G.M.; Huang, D.L.; Feng, C.L.; Hu, S.; Zhao, M.H.; Lai, C.; Wei, Z.; Huang, C.; Xie, G.X., et al. (2012) Use of iron oxide nanomaterials in wastewater treatment: a review. *Sci Total Environ*, 424: 1-10.

(44) Kefeni, K.K.; Msagati, T.A.M.; Mamba, B.B. (2017) Ferrite nanoparticles: Synthesis, characterisation and applications in electronic device. *Materials Science and Engineering: B*, 215: 37-55.

(45) Proposed Selenium Criterion Maximum Concentration for the Water Quality Guidance for the Great Lakes System. In Agency, E.P., Ed. Federal Register, 1996; Vol. 61, pp 58444-58449.

(46) Martínez, M.; Giménez, J.; de Pablo, J.; Rovira, M.; Duro, L. (2006) Sorption of selenium(IV) and selenium(VI) onto magnetite. *Applied Surface Science*, 252(10): 3767-3773.

(47) Tsouris, C.; DePaoli, D.W.; Shor, J.T.; Hu, M.Z.C.; Ying, T.Y. (2001) Electrocoagulation for magnetic seeding of colloidal particles. *Colloids and Surfaces A: Physicochemical and Engineering Aspects*, 177(2-3): 223-233.

(48) Martin-Hernandez, F.; Garcia-Hernandez, M.M. (2010) Magnetic properties and anisotropy constant of goethite single crystals at saturating high fields. *Geophysical Journal International*, 181(2): 756-761.

(49) Tadic, M.; Panjan, M.; Damnjanovic, V.; Milosevic, I. (2014) Magnetic properties of hematite (α-Fe_2O_3) nanoparticles prepared by hydrothermal synthesis method. *Applied Surface Science*, 320: 183-187.

(50) Loyo, R.L.; Nikitenko, S.I.; Scheinost, A.C.; Simonoff, M. (2008) Immobilization of selenite on Fe3O4 and Fe/Fe3C ultrasmall particles. *Environ Sci Technol*, 42(7): 2451-2456.

(51) Lu, A.H.; Salabas, E.L.; Schuth, F. (2007) Magnetic nanoparticles: synthesis, protection, functionalization, and application. *Angew Chem Int Ed Engl*, 46(8): 1222-1244.

(52) Song, X.; Boily, J.F. (2013) Carbon dioxide binding at dry FeOOH mineral surfaces: evidence for structure-controlled speciation. *Environ Sci Technol*, 47(16): 9241-9248.